Preparation, structure, dynamics, and energetics of amorphous silicon: A molecular-dynamics study

W. D. Luedtke and Uzi Landman
School of Physics, Georgia Institute of Technology, Atlanta, Georgia 30332-0430
(Received 23 January 1989)

The preparation of amorphous silicon by molecular-dynamics simulations employing the Stillinger-Weber Si potential, via direct slow cooling from the melt, is described. It is shown that previous failures to obtain amorphous Si using these interaction potentials are of kinetic origin, i.e., related to the quench rate employed. The amorphous silicon sample which we prepared exhibits structural and dynamical properties in good agreement with available experimental data for the static structure factor and phonon density of states. Detailed analyses of the structure, including distributions of bond and dihedral angles and ring statistics, and energetics, including the determination of effective temperatures for n-fold-coordinated atoms ($n=3-5$) and estimates of the formation energy of coordination defects (i.e., $n\neq 4$) are presented. The lack of medium-range order, measured via correlation between dihedral angles associated with adjacent bonds, is discussed.

I. INTRODUCTION

Amorphous materials represent a large area of endeavor in material science on both the basic and technological frontiers.[1-8] The difficulty in studying matter in the amorphous state originates from the lack of periodicity which hinders the use of conventional condensed-matter structural determination and modeling methods. Main issues in studies of amorphous semiconductors (and other amorphous materials) include the structural characterization of these systems which may exhibit a hierarchy of spatial and orientational order (short and intermediate range), the correlations between the structure and the properties of the material and the dependence of the above on the method of preparation. Therefore, efforts have focused on analysis and modeling of the structure of elemental amorphous systems where only positional disorder is present, leading to the development of various models[7,9-13] in which amorphous structures are hand built or computer generated according to well-defined algorithms. Although the above structural models aid the elucidation and interpretation of data, alternative descriptions in terms of interatomic potentials are required in order to investigate the response of materials to changes in external physical conditions and the dynamics and mechanisms of phase transformations (such as melting, crystallization, and amorphization).

Recently, several molecular-dynamics (MD) (and Monte Carlo) simulations of the preparation of amorphous silicon[14-19] (and germanium[20]) via cooling of a melt, employing the Stillinger-Weber[21] (SW) potentials, and other potentials,[19,22] have been performed. While the SW potential, which includes two- and three-body contributions (V_2 and V_3, respectively) and which was parametrized[21] on the basis of solid- and liquid-phase data for Si, yields an adequate description of these aggregation states (bulk,[21] surface phenomena,[23-26] and studies of equilibrium[27,28] and nonequilibrium[29] solid-melt interfaces of silicon), it appears from these studies[14-20] that upon quenching the SW potential produces a range of nearly degenerate disordered structures, and it was suggested that the difference of the configurational entropies of the low-temperature liquid and amorphous phases is in error resulting in a too-small value of the heat of fusion for the liquid to amorphous transition.

In an attempt to alleviate these difficulties, methods for preparing amorphous silicon, using MD simulations and employing the SW potentials, have been developed.[14-18] In one of the preparation procedures which we have explored[17] the system is first prepared at high temperatures and then cooled using an increased three-body potential term, thus enhancing the tendency toward tetrahedral coordination. Once the path which the system traverses in its configuration space has been redirected in this manner, restoring the value of the coefficient (λ) of the three-body potential term to its original SW value[21] ($\lambda=21$) results in an amorphous material which exhibits structural, dynamical, and thermodynamical properties in adequate agreement with experimental data. Furthermore, upon fast heating, the so-prepared amorphous silicon melts via a first-order phase transition at a temperature which is ~ 230 K below the crystalline melting temperature in agreement with experimental measurements. When the behavior of *more fully relaxed* configurations of the amorphous material at several temperatures is analyzed[17] we find that at this effectively slower-heating rate the nature of the transition and the latent heat associated with it are maintained, but melting starts at a lower temperature.

While the amorphous material prepared via the above indirect procedure[17] can be utilized for studies of the properties of the amorphous phase under various conditions, and in investigations of transformations of the amorphous phase, a principal question remains: Do the above documented failures to achieve the amorphous state via *direct quenching of the melt* reflect an *inherent*

defect of the interaction potentials which were employed, *or* is the difficulty of a *kinetic origin*, i.e., related to the quench rates used?

To resolve this question (which is often raised, in various variants, in the context of MD simulations, and in particular those involving nonequilibrium phenomena) we have performed[18] lengthy simulations in which a SW silicon bulk melt was cooled at a rate smaller than has been attempted in all previous MD studies.

Our results demonstrate[18] that the origin of previous failures to obtain amorphous silicon via *direct cooling* of the melt, using the SW potentials, is of kinetic origin. This conclusion may be extended as a general cautionary remark concerning investigations in the area of nonequilibrium phenomena involving phase transformations and "ill-condensed phases" (i.e., amorphous and glassy states).

The method of simulation and the evolution and properties of the amorphous silicon sample thus prepared are described in Sec. II. The results of detailed structural and energetic analysis of the amorphous material, including new techniques for analyzing the simulation data, are presented and discussed in Sec. III.

II. METHOD OF PREPARATION AND PROPERTIES

In our study we have simulated using the MD technique a system of 588 particles interacting via the SW potential employing a three-dimensional periodically replicated calculational cell possessing full dynamical freedom to change shape and volume[30] under zero external pressure, and the equations of motion were integrated using Gear's fifth-order predictor-corrector algorithm with a time step $\Delta t = 1.15\times10^{-3}$ psec. Cooling of the system was achieved by reducing the temperature (via scaling of velocities) at selected stages of the simulation over a $2000\Delta t$ interval by 0.005ϵ ($\epsilon = 50$ kcal/mole) followed by prolonged relaxations at constant energy.

The time evolution of characteristic quantities of the system during the simulation is shown in Fig. 1 [the overall time span is 4.5×10^4 t.u.$=3.447\times10^{-9}$ sec, where the time unit (t.u.)$=7.66\times10^{-14}$ sec. Using the above Δt the complete simulation required about 3×10^6 integration time steps]. As seen from Fig. 1 longer periods of relaxation were required as the temperature of the system decreased (to convert to temperature in degrees Kelvin multiply the reduced temperature by 2.5173×10^4). To demonstrate the slow rate by which the system explores the accessible phase space we show in Fig. 2 the temporal relaxation of system properties for the time span $4.75\times10^3 \le t \le 2.25\times10^4$ t.u. These results serve to emphasize the slow kinetics of relaxation and thus long simulation periods which are required in order to allow a faithful representation of the quenching process.

Results obtained in the present simulations (open circles) for the average total energy E and density ρ versus temperature (in units of the ϵ parameter of the SW potential) during the direct slow quench are given in Fig. 3, along with our previous results[17] for heating of an amorphous silicon system which was prepared via the *indirect* route. For the latter system, results for both a fast-heating (solid line) and a quasistatic-heating process

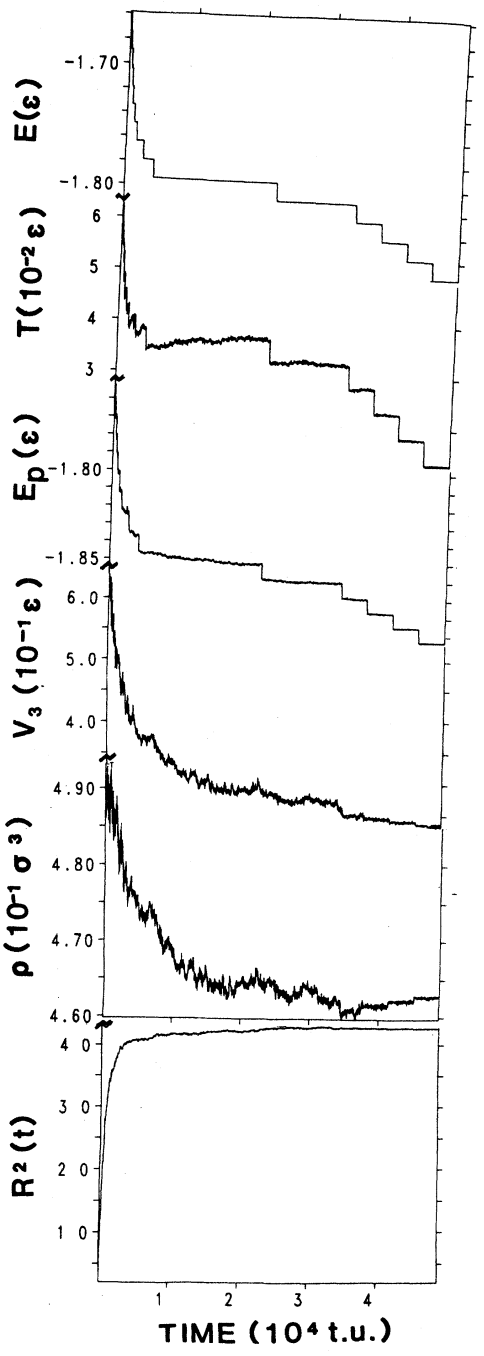

FIG. 1. Total energy (E), temperature (T), potential energy (E_p), three-body potential contribution (V_3), density (ρ), and measure of particles mobility, $R^2(t)=N^{-1}\sum_{i=1}^{N}[\mathbf{r}_i(t)-\mathbf{r}_i(0)]^2$, during the simulation of slowly cooled silicon. Cooling of the system (via scaling of the particles velocities) took place at the times corresponding to the steps most noticeable in the E, T, and E_p plots. Between the cooling steps the system evolves with no temperature control (i.e., constant total energy). Note that different periods of time were required to achieve relaxation during the quench depending on the temperature. $\epsilon = 50$ kcal/mole, density in units of σ^{-3} ($\sigma = 2.0951$ Å), R^2 in units of σ^2, and time in units of t.u.$=7.66\times10^{-14}$ sec.

(solid squares) are shown. As seen, upon cooling the transition from the high temperature is signified by marked sharp changes in the energy and density of the system starting at $T \sim 0.42\epsilon$ (~ 1060 K), followed by a slow variation as cooling continues. We note that, at room temperature, the amorphous silicon system prepared in this study, via slow cooling of the melt, is somewhat denser (Fig. 3) and slightly less fourfold coordinated than the system prepared by us previously[17] via the indirect route (see Table I). The energy per particle in the current system is below that obtained in the previous study (see Fig. 3) and in addition the latent heat for the melt to amorphous transition $\Delta H_{\rm la}$ (estimated from

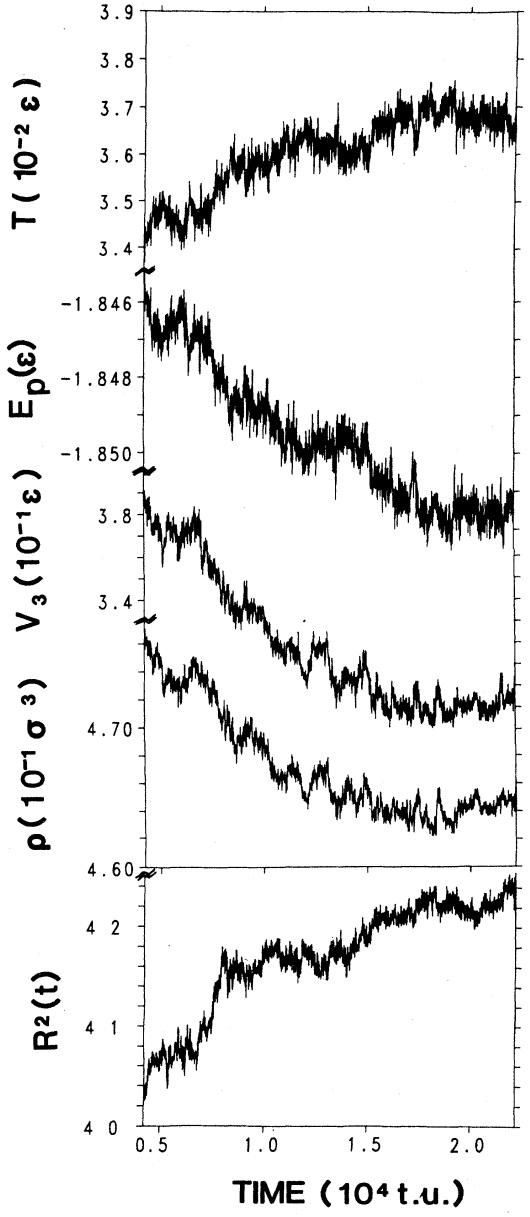

FIG. 2. Same as Fig. 1 for the time interval 4.75×10^3 t.u. $\leq t \leq 2.25\times10^4$ t.u. (i.e., 1.2×10^6 integration time steps) demonstrating the slow-relaxation kinetics.

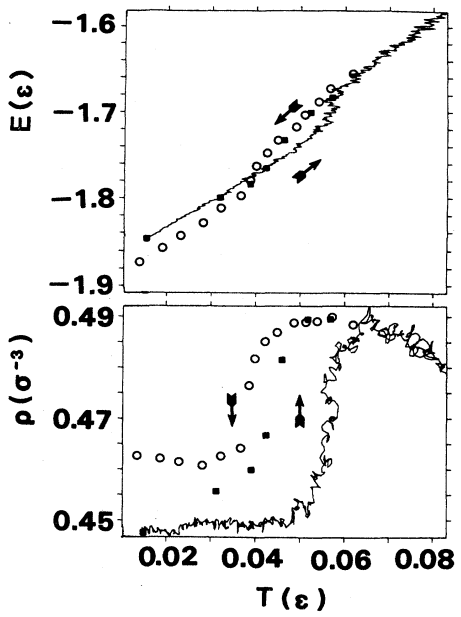

FIG. 3. Total energy per particle E and density ρ of the slowly cooled melt (open circles) and those obtained by heating of the indirectly prepared (Ref. 17) amorphous Si. Solid lines correspond to rapid heating and the solid squares to slow heating allowing for more complete relaxation at the corresponding temperatures, both exhibiting the characteristics of a first-order transition, with melting occurring at a lower temperature for the slow-heating rate.

the energy-versus-temperature data shown in Fig. 3) is larger in the current study ($0.05-0.08\epsilon$ per particle as compared to $0.03-0.06\epsilon$ obtained before[17]). The ratio $\Delta H_{\rm la}/\Delta H_{cl}$, where $\Delta H_{cl}=0.15\epsilon$ is the per-particle latent heat of melting of a SW crystal, is equal to 0.33–0.53 as compared to the 0.2–0.4 obtained by us previously[17] (the experimental estimate for that ratio is ~ 0.67, see Refs. 30 and 31 in Ref. 17).

The quality of the room-temperature amorphous material thus obtained can be assessed from the pair-distribution functions $g(r)$, the density of states $D(\omega)$, and the static structure factor $S(k)$ shown in Figs. 4–6, respectively, and the results given in Table I (where in addition results at ~ 800 K are given). In these figures the results for the amorphous Si material obtained in the present simulation (at 300 K) are denoted by a and those obtained via the indirect route in our previous studies[17] are denoted by a'. In addition, simulation results for the crystalline (c) at 300 K, liquid (l) at the melting point, and glass states of silicon are shown for comparison in Figs. 4 and 5. The results for amorphous Si(a) and Si(a') obtained via the two methods of preparation are very similar and both agree, rather adequately, with available experimental data,[31] except for a shift of the high-frequency peak in the density of states, Fig. 5. The structure factor $S(k)$ (see Fig. 6) calculated[32] from $g(r)$ (Fig. 4) agrees well with that obtained from diffraction data.[32] Having described the method of preparation, thermal his-

TABLE I. Fraction of atoms with given coordination, average bonding angle θ, and its standard deviation and densities (in units of σ^{-3}, $\sigma=2.0951$ Å) for the SW (Ref. 21) amorphous Si obtained by slow cooling in this study (a) and for the indirectly prepared material (Ref. 17) (a') at room temperature (RT) and at $\sim$800 K, as well as for the RT glass and liquid (at the melting point, $T_m=1665$ K). The SW crystal at RT is tetrahedrally coordinated, $C_4=1$, $\theta=109.4\pm2.7$, and $\rho=0.455$. In the bottom part of the table, average bonding angles and their standard deviations corresponding to the various coordinations of sites, are given. In calculating the coordination numbers a cutoff of 2.866 Å was used for the amorphous material at room temperature (RT) and 2.933 Å at $\sim$800 K. For the liquid at T_m a cutoff of 2.933 Å was used. These cutoff values were determined as the first minima in the corresponding pair distributions $g(r)$.

Coordination	a (RT)	a' (RT)	a (810 K)	a' (800 K)	Glass (RT)	Liquid (T_m)
3	0.006	0.007	0.003	0.002	0.002	0.02
4	0.78	0.89	0.71	0.74	0.41	0.29
5	0.21	0.095	0.28	0.24	0.52	0.48
6	0.003	0.001	0.02	0.01	0.07	0.19
7	0	0	0	0	0.001	0.021
average	4.21	4.14	4.31	4.26	4.66	4.89
θ	107.8±16.0	108.4±14.2	107.1±18.3	107.3±18.0	106.6±22.6	103.9±26.8
ρ	0.463	0.448	0.462	0.456	0.489	0.486

Coordination	$\theta(a)$ RT	$\theta(a')$ RT	$\theta(a)$, 810 K	$\theta(a')$, 800 K
3	108.5±14.1	106.1±11.3	110.3±13.0	106.3±12.7
4	109.0±10.25	109.0±11.3	108.9±11.1	108.8±12.0
5	105.2±23.8	105.2±24.6	104.8±24.3	104.8±24.7
6	102.4±29.0	104.0±30.8	101.8±29.1	101.7±29.1

tory, and general properties of the amorphous material which we obtained, we focus in the next section on in-depth analyses of structural and energetic properties of the material.

III. STRUCTURE AND ENERGETICS

We turn now to a detailed analysis of the structural and energetic properties of the amorphous silicon sample Si(a) prepared in this study. From Table I we note that at room-temperature fourfold coordination (C_4) predominates followed by fivefold coordination (C_5) and a much smaller abundance of other coordinations. Furthermore, C_4 decreases and C_5 increases at higher temperature and upon melting $C_5 > C_4$ in the liquid. On the average, fourfold atoms are found to be bonded to three other C_4 atoms and to one C_5 atom, while a fivefold-coordinated atom has on the average 3.5 C_4 neighbors and $\sim$1.4 C_5 neighbors. Furthermore, 36% of the C_4 atoms have only C_4 neighbors, and 38%, 18%, and 6% have exactly 1, 2, and 3 C_5 neighbors, respectively. Similarly, 27% of the C_5 atoms have only C_4 neighbors and 28%, 22%, and 16% have exactly 1, 2, and 3 C_5 neighbors. From the results in Table II we observe that the potential energy (V) per atom is smallest for fourfold-coordinated atoms, due to the much smaller (positive) value of the three-body contribution (V_3) for these atoms. In addition the average bond length d is shorter for C_4-coordinated atoms (Table III).

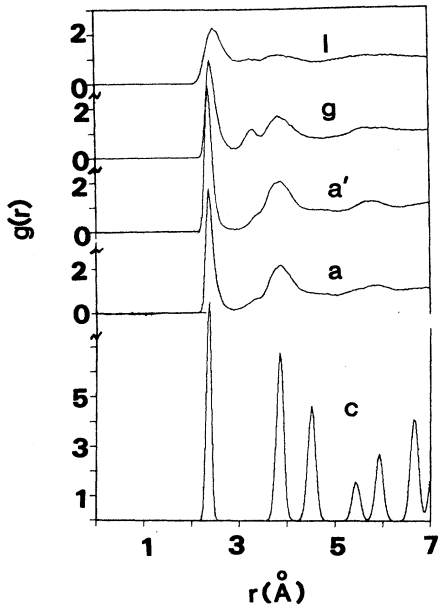

FIG. 4. Radial pair distribution functions $g(r)$: SW Si crystal (c); indirect amorphous (Ref. 17) (a'); slow-quench amorphous sample obtained in this study (a). All at RT. Glass (g) at $T=0.014\epsilon$, and a SW liquid (l) at the melting point ($0.0662\epsilon=1666$ K).

The local pressure in the material can be calculated as one-third of the trace of the contribution due to the ith atom to the stress tensor [see Eq. (7c) in the first paper in Ref. 29, with the volume per atom equal to the total volume of the system divided by the number of atoms]. It is of interest to note (see Table III and Fig. 7) that the average local pressure P associated with C_4-coordinated atoms is slightly positive [i.e., 3.2 kbar, see Fig. 7(b)] while the distribution of local pressures for other coordinated atoms is shifted towards negative pressures indicating an inhomogeneous stress distribution in the material (the overall average internal pressure of the sample is zero, i.e., equal to the external pressure in these constant-pressure simulations). In contrast, near the beginning of the liquid-to-amorphous transition ($T=0.045$,

see Fig. 3) the average pressures of four- and five-coordinated atoms are -12 and 4 kbar, respectively. The signs of these pressures change upon further cooling between $T=0.038$ and 0.037. No further variations in the pressure occur below $T=0.28$ (see Fig. 3). Note in addition the significant width of the pressure distribution in the material. From a plot of the total energy per atom versus pressure [Fig. 7(d)] we observe that for the fourfold-coordinated atoms the smallest energy occurs for those atoms experiencing a local pressure of ~ 16 kbar, while for fivefold-coordinated atoms the minimum energy occurs at a negative value of the local pressure and overall the dependence on pressure is smaller for the latter coordination.

Prior to a detailed discussion of the energetics in the amorphous material we focus on certain structural characteristics. The connectivity of the amorphous net-

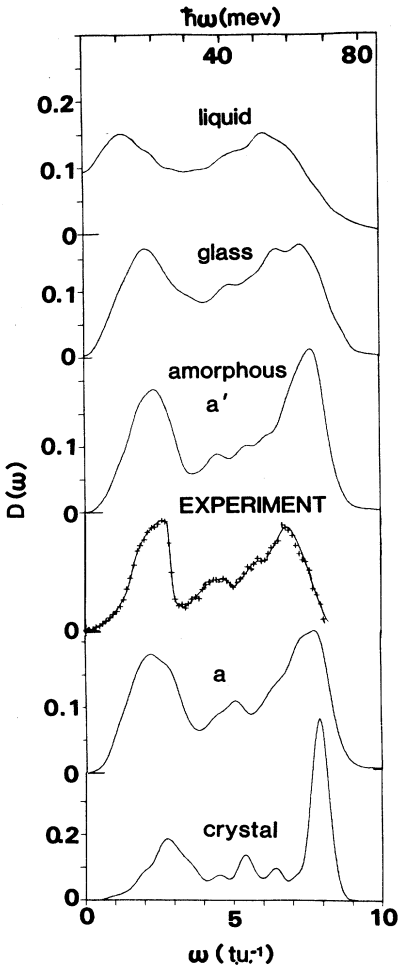

FIG. 5. Density of states $D(\omega)$ for room-temperature SW crystal; indirect amorphous (Ref. 17) (a'); amorphous via slow cooling obtained in this study (a); glass at $T=0.014\epsilon$, and SW liquid at the melting point. Frequency in units of inverse SW time unit (t.u.$=7.66\times10^{-14}$ sec). $D(\omega)$ is normalized such that the integral over ω is unity. The experimental (Ref. 31) $D(\omega)$ is also shown.

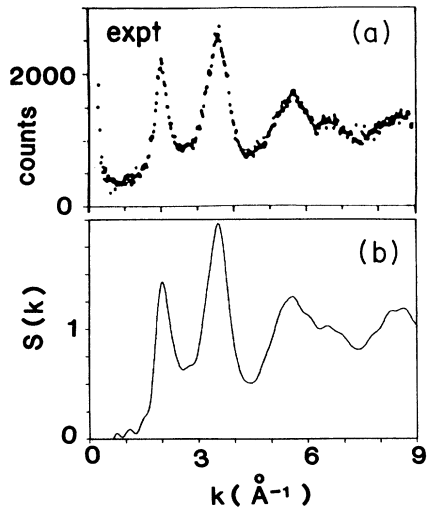

FIG. 6. The static structure factor $S(k)$ (a) from experiment (Ref. 32) and (b) for the amorphous Si obtained in this study. The wave vector k in Å^{-1}.

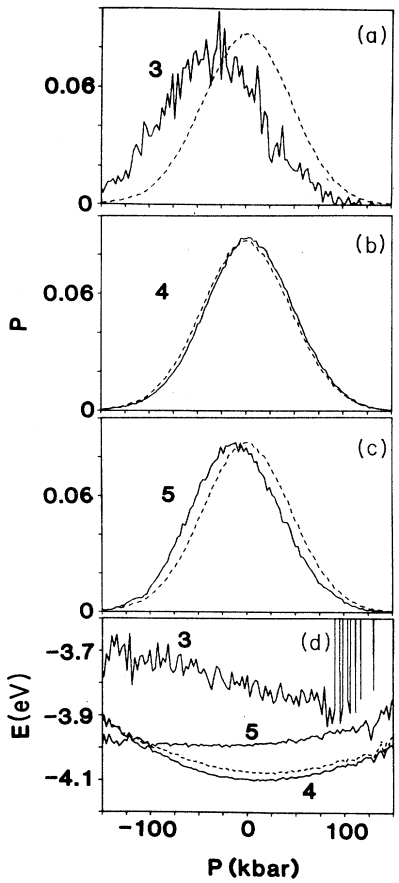

FIG. 7. (a)–(c) Local pressure distribution for three-, four-, and fivefold-coordinated atoms (each normalized to unity). The overall pressure distribution in the sample, peaking at ~ 0, is represented by the dashed line. (d) Total energy (kinetic plus potential) per atom vs local pressure (over a range of ± 150 kbar) for three-, four-, and fivefold-coordinated atoms. The energy vs pressure for the whole sample is represented by the dashed line. Energy in eV, and pressure in kbar.

TABLE II. Per-atom two- and three-body contributions (V_2 and V_3, respectively) to the potential energy and the total potential energy ($V=V_2+V_3$) of n-fold-coordinated atoms in the amorphous Si(a) sample prepared in this study at room temperature. Energies in eV.

Coordination	V_2	V_3	V
3	−4.82±0.36	1.0±0.3	−3.82±0.16
4	−4.48±0.23	0.35±0.28	−4.13±0.12
5	−5.11±0.17	1.10±0.20	−4.03±0.1
6	−5.63±0.20	1.71±0.26	−3.92±0.1
overall	−4.62±0.35	0.51±0.41	−4.10±0.12

work can be analyzed by calculating the average (over the equilibrium ensemble) fraction of bonds, out of the total number of bonds, which connect n- and n'-fold-coordinated atoms [$f(n,n')$] and then calculating the ratio between $f(n,n')$ and that fraction f_{ran} for a random spatial distribution of the n and n' coordination sites. f_{ran} is calculated using the average coordination probabilities $p(n)$ given in Table I (second column), i.e., $f_{\text{ran}}=2p(n)p(n')$ for $n\neq n'$ and $p(n)p(n')$ for $n=n'$, where n and n' denote n and n'-fold-coordinated atoms. As seen from Table IV both four- and fivefold-coordinated atoms are uniformly distributed about fourfold-coordinated atoms. However, fivefold-coordinated atoms tend to be bonded to other fivefold-coordinated atoms. We also observe that the potential energy $V(n,n')$ is lowest for four—four bonds.

Added information about the topology of the amorphous structure is provided by the statistics of rings in the material.[7] These rings (or loops) are constructed by starting from a given atom and tracing a closed path of bonds [defined as two atoms separated by less than $r_c=2.866$ Å, which is the first minimum in the $g(r)$, Fig. 4] with no atoms visited more than once or having bonds to more than two other ring atoms. In the diamond structure of crystalline silicon the smallest ring contains six atoms and there are 12 distinct six-atom rings passing through each atom in the crystal. Each atom of course participates in addition in larger rings. While in perfect crystalline silicon all rings contain an even number of atoms, amorphous Si contains both odd- and even-membered rings as seen from Table V, where the average number of n_r-membered rings to which an atom belongs is given (N_r). As seen, the number of six-membered rings per atom is about half that found in crystalline Si, the most abundant smaller ring is five membered, and seven-membered rings are present along with smaller and larger ones. The average angle χ between neighboring bonds in the rings is also given in Table V and the distributions of χ for three- to six-membered rings are shown in Fig. 8. It is worthwhile noting that the average coordination C of atoms belonging to three-membered rings is five. Furthermore, we observe a marked tendency for fivefold-coordinated atoms in four- and five-membered rings.

From Table I we observe that the average bonding angle θ (i.e., the angle subtended by two bonds emanating from an atom) in the amorphous material is smaller than the tetrahedral angle (109.47°) and that the standard deviation from the mean is large[1,7,33] [16° in the Si(a) sample, at 300 K]. The overall bond-angle distribution $P(\theta)$ and the distributions corresponding to n-fold atoms (normalized to unity in each case) are shown in Fig. 9 (see also Table I). We note that the average bond angle for the fourfold-coordinated atoms is close to the tetrahedral angle and the distribution for these atoms is significantly narrower (±10.25°) than those corresponding to other coordinations. Furthermore we note that the tails at small and large angles and the shoulder at ~80° in the overall angular distribution [Fig. 9(a)] originate from features in $P(\theta)$ for fivefold-coordinated atoms. To further investigate this point we repeat in Fig. 10(a) the angular distribution for C_5 atoms along with a decomposition of that distribution according to the participation of these atoms in three-membered rings. Inspection of these figures reveals that the origin of the features in $P(\theta)$ at ~80° is in the angular distribution of C_5 atoms which do not belong to three-membered rings [Fig. 10(b)] while the feature at low angles (~60°) is due to those C_5 atoms which do participate in three rings [Fig. 10(c)]. The peak at ~80° in Fig. 10(b) also correlates with the shoulder in the pair distribution $g(r)$ in Fig. 4 at $r=3.25$ Å. Added information about the atomic configuration of the

TABLE III. Average bond length d and local pressure P for n-fold-coordinated atoms in the amorphous Si(a) sample at room temperature. Distance in Å and pressure in units of kbar.

Coordination	d	P
3	2.50±0.12	−35.9±51.1
4	2.40±0.09	3.2±46.0
5	2.51±0.13	−10.5±46.3
6	2.61±0.14	−19.3±53.6
overall	2.43±0.10	−0.018±46.51

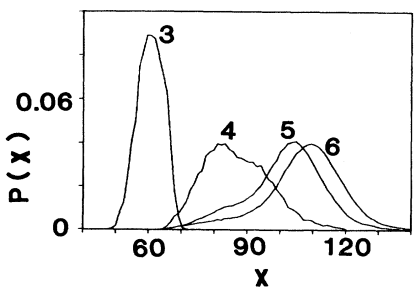

FIG. 8. Distribution of the angle between adjacent bonds $P(\chi)$ in three-, four-, five-, and six-membered rings.

TABLE IV. Bond statistics. The fraction of bonds f connecting n and n'-fold-coordinated atoms, and the ratio between f and that fraction for a random distribution of the atoms. In addition, the dihedral angle ϕ and the per-bond potential energy V (in eV) associated with these bonds are given.

Coordination n	n'	$f(n,n')$	$f(n,n')/f_{\text{ran}}$	$\phi(n,n')$	$V(n,n')$
4	3	0.004	0.38	37.0±13.6	−3.95±0.12
4	4	0.56	0.92	34.0±15.3	−4.13±0.08
4	5	0.36	1.08	27.5±10.1	−4.07±0.08
4	6	0.006	0.60	19.2±9.1	−4.0±0.08
5	3	0.004	0.39	30.6±8.7	−3.95±0.07
5	5	0.07	1.56	25.7±8.8	−4.07±0.08
5	6	0.003	0.31	19.2±6.7	−3.98±0.06

fivefold-coordinated atoms can be obtained from the areas under the peaks in Figs. 10(b) and 10(c). Out of the 10 bond angles we thus estimate that for fivefold atoms with no three rings [Fig. 10(b)] three of the bond angles are close to 80°, which is consistent with a slightly distorted fivefold configuration consisting of a central atom with four neighbors at close to tetrahedral directions and a fifth bond in a direction opposite to one of the other bonds, forming an angle of ~150°–170° with that bond. Since ~73% for the fivefold-coordinated atoms do not participate in three-membered rings, the above configuration is the most prevalent one.

A higher-order angular characteristic of a covalent network is the distribution of dihedral angles which together with the ring statistics discussed above allows analysis of medium-range order (MRO),[1,7,34,35] beyond the short-range order (SRO) probed via the pair-distribution function $g(r)$ and bond-angle distribution $P(\theta)$. However, while SRO is usually observed from diffraction measurements, no general experimental technique is currently available which provides a *direct* measure[34,35] of quantities pertinent to determination of MRO, except in certain favorable cases using Raman spectroscopy.[1,34,36–39] It is therefore of particular interest to explore the degree and consequences of MRO in the amorphous silicon sample which we have modeled.

The dihedral angle ϕ measures the relative disposition of a pair of bonds that are *not* adjoining but that both adjoin a common intervening bond (the "central bond"). It is constructed[7] by projecting onto the plane which perpendicularly bisects the bond joining a pair of nearest-neighbor atoms, the other bonds that are attached to each of the two atoms connected by the central bond. The dihedral angle is computed as the average angle between a bond projection belonging to one atom from the nearest bond projection belonging to the other atom. In a tetrahedrally bonded network ϕ ranges between 0° (eclipsed configuration) and 60° (staggered configuration).

TABLE V. Ring statistics. Number of atoms in a ring n_r; average number of rings of type n_r passing through an atom N_r; average coordination C of atoms making up rings of type n_r; average bond angles χ in rings of type n_r; average dihedral angle ϕ associated with the bonds belonging to rings of type n_r. The average potential energy per ring atom is smallest for six-membered rings and is ~ −4.1 eV for all ring types.

n_r	N_r	C	χ	ϕ
3	0.06	5.0±0.1	60.0±0	23.1±5.7
4	0.3	4.6±0.2	86.4±3.4	26.6±6.2
5	3.1	4.3±0.2	101.1±3.7	30.9±5.2
6	6.6	4.25±0.2	106.8±4.5	34.1±5.5
7	9.0	4.25±0.2	108.8±4.6	32.0±4.5
8	13.7	4.3±0.2	109.7±4.6	31.9±5.2

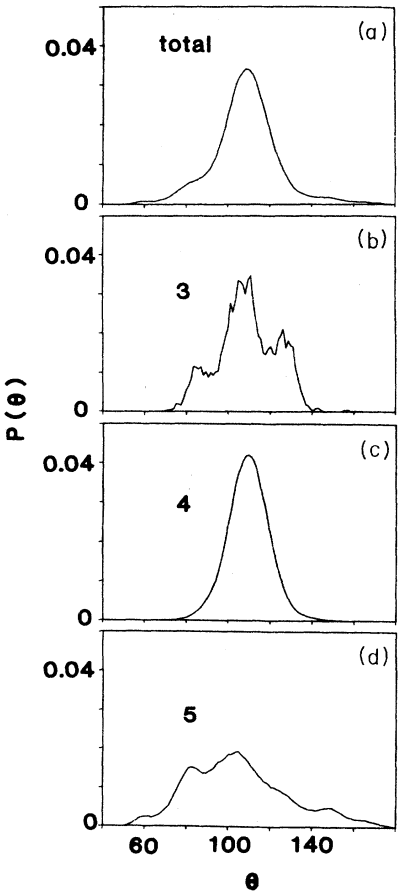

FIG. 9. Bond-angle distributions $P(\theta)$. (a) Overall distribution for the amorphous Si(a) sample. (b)–(d) $P(\theta)$ distributions for three-, four-, and fivefold-coordinated atoms (each normalized to unity), respectively.

In crystalline diamond only the staggered configuration appears, while the tetrahedral continuous random network[7] (CRN) is characterized by a continuous distribution of dihedral angles, extending monotonically from 0° to 60°.

The overall, normalized, dihedral angle distribution $P(\phi)$ in our amorphous silicon is exhibited in Fig. 11(a) and a decomposition of $P(\phi)$ into contributions (each normalized to unity) from four—four, five—five, and four—five bonds (where n—n' refers to the coordination numbers of the atoms defining the central, adjoining bond) is given in Figs. 11(b)–11(d), respectively. The average value of ϕ in our sample is $32.2°\pm13.5°$ with a marked feature at $\phi > 40°$ [see Fig. 11(a)] which originates from the dihedral angle associated with bonds between fourfold-coordinated atoms [see Fig. 11(b)]. We note that the peak in Fig. 11(b) at $\phi \sim 50°$ indicates that the staggered configuration is favored relative to the eclipsed one for adjoining tetrahedra. In addition the average and standard deviation of $\phi(n,n')$ associated with bonds between n and n'-fold-coordinated atoms are given in Table IV, and the average ϕ values characterizing the bonds in n_r-membered rings are given in Table V.

It is of interest to explore the energetic consequences of the dihedral angle distribution. In Fig. 12(a) the average per-atom potential energy for the atoms defining the bond between two adjoining polyhedra versus ϕ is shown, indicating an energetic preference at the two limits of the dihedral angle range (corresponding to eclipsed and staggered configurations in case of two adjoining tetrahedra), and an insensitivity to ϕ otherwise. The decomposition of the overall distribution according to the coordination of the adjoint atoms defining the central bond, given in Figs. 12(b)–12(d), shows the bond energies of five—five and four—five bonds to be higher and less correlated to the dihedral angle than four—four bonds.

Since the dihedral angle measures the relative orientation of adjoining polyhedra, correlations *between* dihedral angles (i.e., the phase relationship between pairs of dihedral angles) can serve as a measure of MRO in the material.[34,35] The average sum (P_s) and difference (P_d) between two dihedral angles calculated for two central bonds which emanate from a common atom can serve as an elementary order parameter of such a correlation. The overall P_s and P_d distributions versus angle calculated for our sample are shown in Figs. 13(a) and 13(b) (solid line) as well as those for a random distribution (dashed line) calculated by using the overall dihedral distribution $P(\phi)$ [see Fig. 11(a)], according to

$$P_s(\phi)=\int_0^{\pi/3} P(\phi')P(\phi-\phi')d\phi' , \tag{1}$$

and

$$P_d(\phi)=2\int_0^{\pi/3} P(\phi')P(\phi+\phi')d\phi' . \tag{2}$$

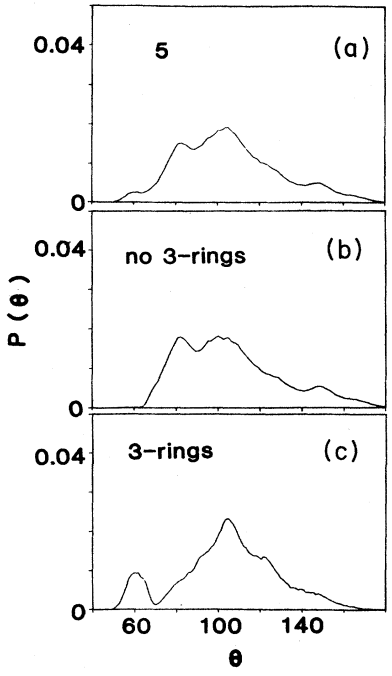

FIG. 10. Bond-angle distributions $P(\theta)$ for fivefold-coordinated atoms. (a) Total $P(\theta)$; (b) $P(\theta)$ for fivefold-coordinated atoms participating in no three-membered rings; (c) $P(\theta)$ for fivefold-coordinated atoms which participate in three-membered rings.

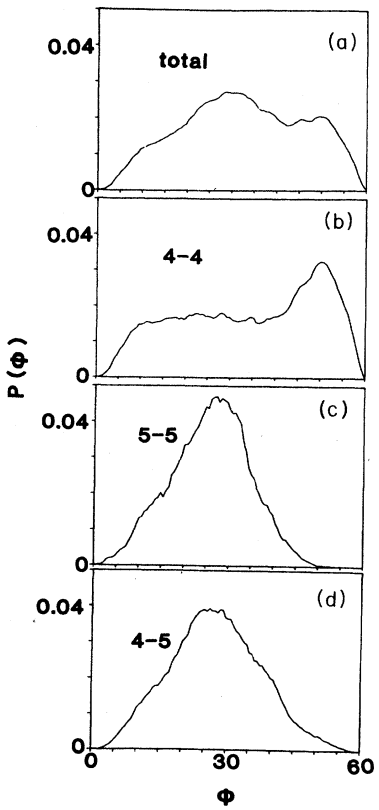

FIG. 11. Dihedral-angle distribution $P(\phi)$. (a) Overall distribution for the amorphous Si(a) sample. (b)–(d) $P(\phi)$ distributions for central bonds connecting fourfold-fourfold–, fivefold-fivefold–, and fourfold-fivefold–coordinated atoms (each normalized to unity), respectively.

Since $P_d(\phi)$ is symmetric about zero, only the positive angle range needs to be considered and thus a prefactor of 2 was inserted in Eq. (2) for proper normalization.

For a Si crystal (diamond structure) the P_s and P_d distributions are narrowly peaked about $\sim 120°$ and 0°. The distributions for the amorphous sample (solid line) and for the calculated random distributions both peak at $\sim 60°-70°$ (P_s) and 0° (P_d) and are much broader than the crystalline ones. The similarity between the P_s and P_d distributions for the simulated amorphous material and the calculated random ones indicates a lack of correlation[1] between neighboring dihedral angles as measured by this order parameter. The same conclusion is drawn from the P_s and P_d distributions shown in Fig. 14 which are calculated for a restricted set of dihedral angle, i.e., those in which the two central bonds adjoin fourfold-coordinated atoms only.

Having discussed in detail the structural properties of the amorphous Si prepared in our simulations we turn next to an analysis of certain energetic aspects of the material. Following a recent analysis[19] we show in Fig. 15 the overall (dashed line) distribution $P(E)$ of atom potential energies and a decomposition into distributions for three-, four-, and fivefold-coordinated atoms (each normalized to unity; for the relative weights see Table I). In these calculations neighbors are defined within a cutoff radius of 2.866 Å [the first minimum in $g(r)$, Fig. 4] and while the two-body interaction energy is divided equally between the bonded atoms, the three-body interaction is assigned to the vertex atoms.[19] The same results, plotted on a logarithmic scale are shown in Fig. 16. As seen from Fig. 15 the overall $P(E)$ peaks at ~ -4.15 eV, cuts off at ~ -4.325 eV [close to the lowest energy (-4.33 eV) in the potential energy distribution calculated for a SW silicon crystal at 300 K] and possesses a high-energy tail. The distributions for differently coordinated atoms peak at different energies, lowest for the fourfold-

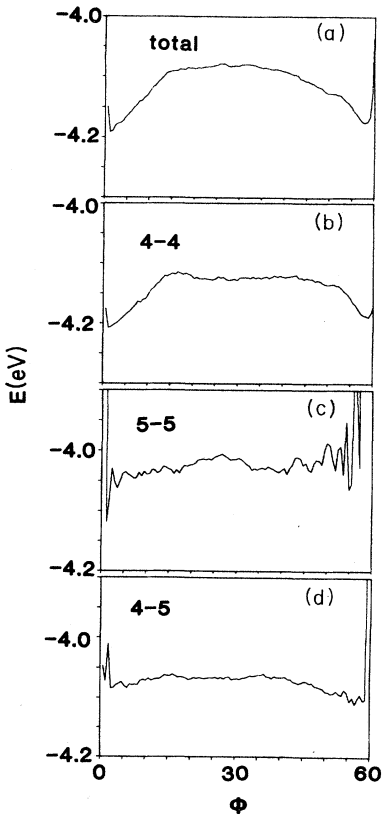

FIG. 12. Per-atom potential energy for atoms defining the central bond vs the dihedral angle ϕ associated with the bond. (a) For the whole sample and (b)–(d) decomposition according to the coordinations of the adjoining atoms defining the central bond; four—four, five—five, and four—five (b)–(d), respectively. Energy in eV.

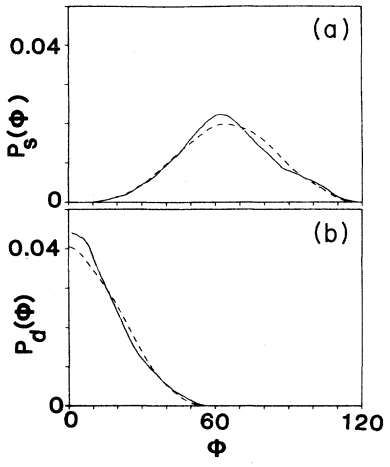

FIG. 13. Distributions of the sum P_s and difference P_d of dihedral angles calculated for pairs of dihedral angles associated with two central bonds which emanate from a common atom. Data for the simulated amorphous Si(a) sample are represented by the solid line and the distributions for random orientations [see Eqs. (1) and (2)] by dashed lines. The similarity between the results of our simulations and the constructed random-orientation distributions indicates the lack of medium-range order (MRO) in our sample, as measured by these order parameters.

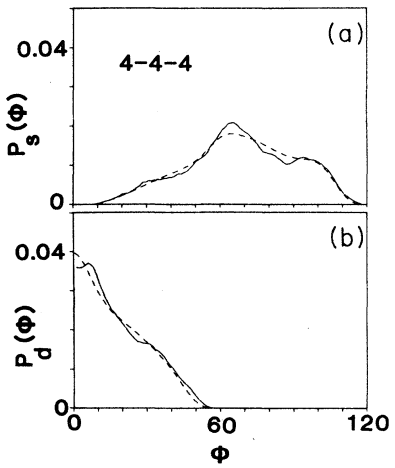

FIG. 14. Same as Fig. 13 but calculated for pairs of central bonds defined by fourfold-coordinated atoms.

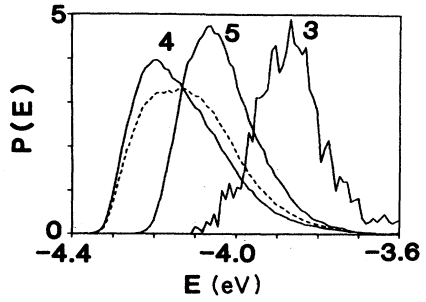

FIG. 15. Per-atom potential energy distribution $P(E)$ for the amorphous Si(a) sample. The dashed line represents the total distribution for the sample. Individual distributions (each normalized to unity) for three-, four-, and fivefold-coordinated atoms are represented by the solid lines, and are identified by the labels. Energy in eV.

coordinated and highest for the threefold-coordinated atoms. The logarithmic plots of $P(E)$ shown in Fig. 16 show that the high-energy tails vary as exponential Maxwell-Boltzmann distributions over several decades. Analysis of the slopes of the high-energy tails yields the effective temperatures $T^*=1008$ K ($=0.04\epsilon$), $T_3^*=840$ K ($=0.0334\epsilon$), $T_4^*=1061$ K ($=0.0421\epsilon$), and $T_5^*=806$ K ($=0.032\epsilon$), for the overall and three-, four-, and fivefold coordinations (Fig. 16), respectively (the values in parentheses give the temperature in units of ϵ of the Stillinger-Weber potential). Due to the poor statistics for threefold-coordinated atoms the value for T_3^* is only a crude estimate. Note that all of the above effective temperatures are much higher than the actual temperature of our sample (300 K), and show an overall similar trend to that obtained in a previous study[19] in which a different interaction potential and method of preparation were employed.

The effective temperature can be interpreted as corresponding to that temperature below which the amorphous network freezes, i.e., significant atomic mobility ceases, except for defects which remain mobile down to lower temperatures and whose mobility may occur via mechanisms which do not involve significant spatial-atomic displacements.[40,41] Consequently, the quenched amorphous material seems to exhibit quasiequilibrium thermal distributions at effective temperatures T_n^* (where

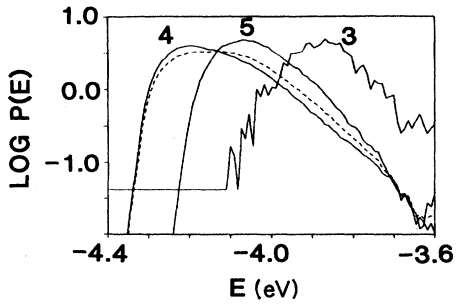

FIG. 16. Same as Fig. 15, but for $\log_{10}P(E)$. The effective temperatures $T_n^*(n=3-5)$ are obtained from the straight-line portions of the high-energy tails of these curves.

n denotes the local coordination) corresponding to the various local geometries in the amorphous network.[19] Indeed we note that the calculated value of T_4^* is close to the temperature at which the transition from liquid to amorphous silicon commences during our slow quench (see Fig. 3) and the value of T_5^* corresponds to the temperature where most of the transformation has taken place (i.e., fivefold-coordinated atoms maintain their mobility down to T_5^*) and only small variations in the amorphous system properties (see density in Fig. 3) occur below that temperature. The value of the overall T^* for the system coincides with the temperature at the middle of that transition.

The significance of the concept of effective temperature is that it relates to kinetic stages in the formation of the amorphous network which may also correspond to the relatively low temperatures at which coordination defects (i.e., three- and fivefold coordinations) may be annealed.[19,42] Additionally, the significance of T^* in determining the electronic band tails and the defect type and concentration in amorphous semiconductors has been discussed.[43]

Finally, following the mode of analysis suggested in Ref. 19 we estimate coordination-defect formation energies [$E_d(n)$, where n is the coordination] in our simulated amorphous silicon. To estimate $E_d(n)$ we calculate for each n-fold-coordinated atom the potential energy of the cluster of $n+1$ atoms consisting of the atom and its n neighbors. From this energy, we subtract the potential energy of $n+1$ fourfold-coordinated atoms, which thus serves as an estimate of the potential energy in a tetrahedrally bonded environment. The potential energy (per atom) in a tetrahedrally coordinated environment used as reference can be calculated either by including in the calculation (of the energy of the 4+1 atom clusters) only those fourfold-coordinated atoms which are bonded to other fourfold-coordinated atoms or by including all C_4 atoms with no distinction of the coordinations of the neighbors. The distribution for the former case peaks at -4.156 eV and for the latter one -4.137 eV. The formation energy distributions shown in Fig. 17 correspond to the second choice, which for fourfold coordination yields a $P(E_d)$ distribution peaking at zero energy, by

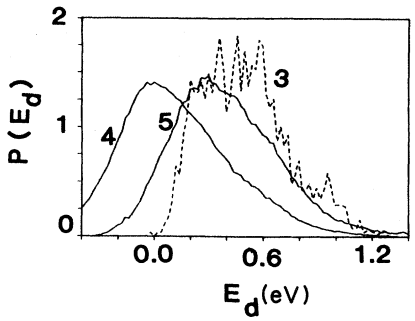

FIG. 17. Distribution of "formation energies" for three-, four-, and fivefold-coordinated atoms, defined relative to fourfold-coordinated atoms (see text). The data for threefold-coordinated atoms (dashed line) are "noisy" due to poor statistics. Energy in eV.

definition. Use of the alternative reference results in a rigid shift of 0.095 eV to higher energy of the fourfold coordination $P(E_d)$, and shifts by 0.08 and 0.114 eV of the $P(E_d)$ for three- and fivefold coordinations, respectively.

From the data shown in Fig. 17 we obtain a formation energy of 0.45 and 0.3 eV for three- and fivefold-coordinated defects, respectively. The value for $E_d(n=5)$ is in agreement with that calculated in Ref. 19 for the SW potential, and for $E_d(n=3)$ our value is somewhat lower (however, this value should be regarded only as a crude estimate due to poor statistics of the threefold-coordinated atoms). While no experimental values are available for these formation energies, they are in the range of estimated values.[41,43]

ACKNOWLEDGMENTS

This work was supported by the U.S. Department of Energy (DOE) under Grant No. DE-FG05-86ER45234. The computations were performed on the Cray Research, Inc. X-MP/48 computer at the National Magnetic Fusion Energy Computer Center, Livermore, California. Helpful discussions with R. N. Barnett and C. L. Cleveland are gratefully acknowledged.

[1]J. S. Lannin, Phys. Today **41(7)**, 28 (1988).
[2]*Amorphous Semiconductors,* edited by M. H. Brodsky (Springer, Berlin, 1985).
[3]*Tetrahedrally-Bonded Amorphous Semiconductors,* edited by D. Adler and H. Fritzsche (Plenum, New York, 1985).
[4]*Amorphous Materials: Modeling of Structure and Properties,* Conference Proceedings of the Metallurgical Society of AIME, edited by V. Vitek (AIME, New York, 1983).
[5]*Amorphous and Liquid Semiconductors,* edited by J. Stuke and W. Brenig (Taylor and Francis, London, 1974).
[6]*Disordered Semiconductors,* edited by M. Kastner and G. A. Thomas (Plenum, New York, 1987).
[7]R. Zallen, *The Physics of Amorphous Solids* (Wiley, New York, 1983).
[8]N. E. Cusack, *The Physics of Structurally Disordered Matter* (Adam Hilger, Bristol, 1987), Chap. 11.
[9]D. E. Polk, J. Non-Cryst. Solids **5**, 365 (1971).
[10]M. G. Duffy, D. S. Boudreaux, and D. E. Polk, J. Non-Cryst. Solids **15**, 435 (1974).
[11]D. Henderson and F. Herman, J. Non-Cryst. Solids **8-10**, 359 (1972); D. Henderson, *ibid.* **16**, 317 (1974).
[12]L. Guttman, Phys. Rev. B **23**, 1866 (1981).
[13]F. Wooten, K. Winer, and D. Weaire, Phys. Rev. Lett. **54**, 1392 (1985).
[14]J. Q. Broughton and X. P. Li, Phys. Rev. B **35**, 9120 (1987).
[15]M. D. Kluge, J. R. Ray, and A. Rahman, Phys. Rev. B **36**, 4234 (1987).
[16]R. Biswas, G. S. Grest, and C. M. Soukoulis, Phys. Rev. B **36**, 7437 (1987).
[17]W. D. Luedtke and U. Landman, Phys. Rev. B **37**, 4656 (1988).
[18]See U. Landman and W. D. Luedtke, in *Atomistic Modeling in Materials: Beyond Pair-Potentials,* edited by V. Vitek (Plenum, New York, 1988).
[19]P. C. Kelires and J. Tersoff, Phys. Rev. Lett. **61**, 562 (1988).
[20]K. Ding and H. C. Andersen, Phys. Rev. B **34**, 6987 (1986).
[21]F. H. Stillinger and T. A. Weber, Phys. Rev. B **31**, 5262 (1985).
[22]R. Car and M. Parrinello, Phys. Rev. Lett. **60**, 204 (1988).
[23]F. F. Abraham and I. P. Batra, Surf. Sci. **163**, L752 (1985).
[24]F. F. Abraham, I. P. Batra, and S. Ciraci, Phys. Rev. Lett. **60**, 1314 (1988).
[25]U. Landman, W. D. Luedtke, and A. Nitzan, Surf. Sci. **210**, L177 (1989).
[26]U. Landman, W. D. Luedtke, and M. W. Ribarsky, J. Vac. Sci. Technol. (to be published).
[27]U. Landman, W. D. Luedtke, R. N. Barnett, C. L. Cleveland, M. W. Ribarsky, E. Arnold, S. Ramesh, H. Baumgart, A. Martinex, and B. Khan, Phys. Rev. Lett. **56**, 155 (1986).
[28]F. F. Abraham and J. Q. Broughton, Phys. Rev. Lett. **59**, 64 (1987).
[29]U. Landman, W. D. Luedtke, M. W. Ribarsky, R. N. Barnett, and C. L. Cleveland, Phys. Rev. B **37**, 4637 (1988); **37**, 4647 (1988); see also U. Landman, in *Computer Simulation Studies in Condensed Matter Physics: Recent Developments,* edited by D. P. Landau, K. K. Mon, and H.-B. Schuttler (Springer, Berlin, 1988).
[30]M. Parinello and A. Rahman, Phys. Rev. Lett. **45**, 1196 (1980).
[31]W. A. Kamitakahara, C. M. Soukoulis, H. R. Shanks, U. Buchenau, and G. S. Grest, Phys. Rev. B **36**, 6539 (1987).
[32]T. A. Postal, C. M. Falco, R. T. Kampwirth, I. K. Schuller, and W. B. Yelon, Phys. Rev. Lett. **45**, 648 (1980).
[33]J. S. Lannin, J. Non-Cryst. Solids **97**, 39 (1987).
[34]G. Lucovsky, J. Non-Cryst. Solids **97**, 155 (1987).
[35]S. R. Elliott, J. Non-Cryst. Solids **97**, 159 (1987).
[36]L. J. Pilione, R. J. Pomian, and L. S. Lannin, in *Optical Effects in Amorphous Semiconductors (Snowbird, Utah),* Proceedings of the Conference on Optical Effects in Amorphous Semiconductors, AIP Conf. Proc. No. 120, edited by P. C. Taylor and S. G. Bishop (AIP, New York, 1984), p. 386.
[37]R. Tsu *et al.*, J. Phys. (Paris) Colloq. **42**, C4-269 (1981).
[38]F. L. Galeener, Solid State Commun. **44**, 1037 (1982).
[39]G. Lucovsky and F. L. Galeener, J. Non-Cryst. Solids **37**, 53 (1980).
[40]S. T. Pantelides, Phys. Rev. Lett. **57**, 2979 (1986).
[41]S. T. Pantelides, Phys. Rev. B **36**, 3479 (1987).
[42]D. V. Lang, J. D. Cohen, and J. P. Itarbison, Phys. Rev. Lett. **48**, 421 (1982).
[43]Y. Bar-Yam, D. Adler, and J. D. Joannopoulos, Phys. Rev. Lett. **57**, 467 (1986).